GEODESY AND CARTOGRAPHY
Vol. 60, No 1, 2011, pp. 35-59

Analysis of some low- and high-dynamics errors of Low-Cost *IMU*

Krzysztof K. Vorbrich

Astrogeodynamical Observatory
Space Research Centre, Polish Academy of Sciences
Borowiec, 4 Drapałka St., 62-035 Kórnik, Poland
e-mail: vorb@cbk.poznan.pl

Received: 2 July 2010 /Accepted: 6 March 2011

Abstract: The paper expounds relevant results of some of the present author's experiments defining the strapdown *IMU* sensors' errors and their propagation into and within *DGPS/IMU*. In order to deal with this problem, the author conducted both the laboratory and field-based experiments.

In the landborne laboratory the stand-alone Low-Cost *IMU* MotionPak MKII was verified in terms of the accelerometer bias, scale factor, gyroscope rotation parameters and internal temperature cross-correlations.

The waterborne field-trials based on board dedicated research ships at the lake and at the busy small sea harbour were augmented by the landborne ones. These experiments conducted during the small, average, and high dynamics of movement provided comparative sole-*GPS*, stand-alone *DGPS* and integrated *DGPS/IMU* solution error analysis in terms of the accuracy and the smoothness of the solution. This error estimation was also carried on in the context of the purposely-erroneous incipient *DGPS/IMU* initialisation and alignment and further in the circumstances of on-flight alignment improvement in the absence of the signal outages.

Moreover, the lake-waterborne tests conducted during extremely low dynamics of movement informed about the deterioration of the correctly initialised *DGPS/IMU* solution with reference to the stand-alone *DGPS* solution and sole-*GPS* solution.

The above-mentioned field experiments have checked positively the *DGPS*/MKI research integrating software prepared during the Polish/German European Union Research Project and modified during the subsequent Project supported by the Polish Committee for Scientific Research.

Keywords: *IMU, INS*, *MEMS, [D]GPS/IMU*, Kalman filter, waterborne & landborne tests

1. Introduction

In the Space Research Centre of the Polish Academy of Sciences (SRC) the theoretical analyses and the experiments with the *IMU* and *INS* have been carried on since the early 1990's. The applicability of this experience to the research on the space-vehicle became evident in 2007 when the SRC started cooperation with the Institute of Space Physics

in Italy on the BepiColombo Mercury Mission and the Italian Space Accelerometer. The above defines the fundamental reasons for the report included below.

The paper strives to answer the question on the applicability of various experimental techniques for testing dynamics-dependent accuracy of *IMU* MEMS MKI, MKII, and *[D]GPS*/MKI.[1]

In the first experimental section the paper provides a simple method of the preliminary laboratory testing of the MKII's accelerometer's errors using the gravity vector **g** as a reference, cf. (Lawrence, 1993; Titterton and Weston, 2004).

In the second experimental section the paper describes some of the *IMU* and *INS* error testing against the reference constituting the following simultaneous solutions: integrated *[D]GPS/*MKI, stand-alone *[D]GPS*, and sole-*GPS*, cf. procedures reported in (Grejner-Brzezinska, 2005).[2]

The physical/chemical properties of MKI and MKII leading to the positive short--term qualities are widely known, cf. (Everett, 1995, p. 393; Wang, 1996, p. 54). The technical and mathematical-exactitude properties of the stand-alone MKI and MKII are broadly recognized throughout the researchers' fraternity, cf. (AAS, 2005, pp. 343, 344).

In scientific applications since the beginning of this century MotionPak has been probably most frequently used in the research on manned vehicle-based-mapping and unmanned-robotics. For the first mentioned application cf. for example: (Valldorf and Gessner, 2005, p. 509). The last mentioned applications are usually land-/waterborne ones. For the landborne robots bearing MotionPak cf. (Caccia et al., 2008).

However, there is no reason why MotionPak-like *IMU* could/should not be mounted on board robots dedicated for the surface of Mars or Mercury, cf. (Fontaine et al., 2009; Novara, 2001).

The waterborne robots bearing MotionPak included Autonomous Underwater Vehicles (AUVs). Regarding AUVs, cf. (Wang, 1996, p. 37). MotionPak was also used in the seismic hardware setup, cf. (Teisseyre et al., 2006, p. 158). For the geodetic applications of the integrated satellite/Low-Cost-*IMU*, cf. (Grejner-Brzezinska, 2005).

Probably in most of the scientific projects mentioned the crucial factor of MotionPak applicability was its response to very-low and/or very-high dynamics. The paper strives to answer the question on the applicability of various experimental techniques for testing MKI's and MKII's dynamics-dependent accuracy. The dynamics dependence of the *IMU* errors' behaviour has been very well explained in (Titterton and Weston, 2004). With regard to the testing of the dynamics-dependence of MKII and other MEMS Inertial Sensors ISs it is worthwhile to consult: (AAS, 2005, p. 343).

According to the contemporary literature the highest growth potential for the investigation on the MEMS accelerometers appears in the research for the automo-

[1] MEMS – Micro-Electro-Mechanical Systems, cf. (Lobontiu and Garcia, 2005). For more information on the Systron Donner's MotionPak^{TM} Mark I (MKI) and Mark II (MKI) cf. (Systron Donner Inertial, 2008).

[2] The [*D*] stands for the optionally Differential *GPS*. The sign / means "software-only Kalman filter integration".

tive applications. Some of these require comparatively very small errors and small noise in the accelerometer's zero-g dynamics and the immunity to vibrations and to the parasitic high frequency content present in the car's chassis, for example for the Electrical Parking Brake (EPB), cf. (Reze and Hammond, 2005, pp. 461, 469, 470).

However, the integrating *DGPS/*MKI software and the testing techniques presented in the paper had in mind the scientific land- and waterborne geodetic (Grejner-Brzezinska, 2005), and hydrography and oceanography application.

The paper checks and explores the opportunities provided by the *[D]GPS*/MKI system with the open-code research Kalman filter driven software designed during the EU Research Programme.

2. Theoretical background for the error equations for *IMU* and *[D]GPS/IMU*

2.1. IMU sensor error compensation

Meticulous *IMU* laboratory testing is necessary for the determination of the coefficients of the error equations, which are prerequisite for the optimal *IMU & INS* error propagation tuning.

2.1.1. Fundamental error equations of the accelerometer and gyro

Below are presented simplified Inertial Sensors' error equations applicable in the laboratory. The following systems of coordinates are mentioned below: body system "b", cf. (Titterton and Weston, 2004, p. 22). Inertial System of Coordinates ISC or "i", cf. (Jekeli, 2001, p. 5, and passim). In ISC the Newton's Equivalence Principle (NEP) is valid. Semi-Inertial System of Coordinates (SISC), definition see (Jekeli, 2001, p. 5). For a definition of "b" and SISC frames with reference to ISC see (Jekeli, 2001, p. 25; Titterton and Weston, 2004, p. 24).

The observations and measurements provided by the Z-axis accelerometer, may be expressed in one of the simplest possible vector forms as follows:

pure inertial case:

$$\mathbf{a}_{Z0} = S_{aZacc}\,\mathbf{a}_Z + \mathbf{B}_{Zacc} + \mathbf{n}_{Zacc} \tag{1a}$$

pure gravitational case:

$$\mathbf{g}_{Z0} = S_{gZacc}\mathbf{g}_Z + \mathbf{B}_{Zacc} + \mathbf{n}_{Zacc} \tag{1b}$$

mixture of inertial and gravitational case:

$$\aleph_{Z0} = S_{\aleph Zacc}\aleph_Z + \mathbf{B}_{Zacc} + \mathbf{n}_{Zacc} \tag{1c}$$

where above: we neglect the influence of the Earth's rotation, and further: $\mathbf{a}_{Z0}, \mathbf{g}_{Z0}, \aleph_{Z0}$ – output of the Z-axis accelerometer; $\mathbf{a}_Z, \mathbf{g}_Z, \aleph_Z$ – input along Z-axis accelerometer;

$S_{aZacc}, S_{gZacc}, S_{\aleph Zacc}$ – scale factor pertaining respectively to magnitudes of: $\mathbf{a}_Z, \mathbf{g}_Z, \aleph_Z$ (Input/Output (I/O) function is presumed to be symmetrical with reference to the Output axis); $\mathbf{B}_{Zacc}$ – gravitation g independent acceleration measurement bias, pertaining to the Z-axis accelerometer; $\mathbf{n}_{Zacc}$ – accelerometer zero-mean random bias.

In the 3D ISC or "i" the component $\aleph_{Z0}$ sensed by the Z-axis accelerometer will be as follows:

$$\aleph_{Z0i} = \mathbf{a}_{Z0i} + \mathbf{g}_{Z0i} \tag{2}$$

Similarly, the measurements $\bar{\boldsymbol{\omega}}_{Z0}$ provided by a Z-axis gyroscope of the *IMU* triad may be expressed in rudimentary vector form as follows (allowance has been made for the Earth rate component):

$$\bar{\boldsymbol{\omega}}_{Z0} = S_{\varpi Zgyro}\bar{\boldsymbol{\omega}}_Z + \mathbf{B}_{Zgyro} + \mathbf{n}_{Zgyro} \tag{3}$$

where: $\bar{\boldsymbol{\omega}}_{Z0}$ – output of the Z-axis gyroscope; $\bar{\boldsymbol{\omega}}_Z$ applied gyration components acting along gyro's Z-rotation axis (input); $\bar{\boldsymbol{\omega}}_{Z0}, \bar{\boldsymbol{\omega}}_Z$ have magnitudes of the angular rotation, and have "senses" in terms of the clock-wise (CW, positive) or anti-clockwise (ACW, negative) rotation along the Z-rotation axis; $S_{\varpi Zgyro}$ – scale factor pertaining to the Z-axis gyroscope and the magnitude $\bar{\boldsymbol{\omega}}_Z$; $\mathbf{B}_{Zgyro}$ – gravitation g insensitive Z-gyro measurement bias; $\mathbf{n}_{Zgyro}$ Z-axis gyro zero-mean random bias.

Further instead of $S_{aZacc}, S_{gZacc}, S_{\aleph Zacc}$, and $S_{\varpi Zgyro}$ we will here write S_{Zacc}, S_{Zgyro} respectively. In (1a), (1b), (1c), (2), and (3) no allowance has been made for cross sampling coefficients, gravity dependent biases, and the drift errors, cf. (Lawrence, 1993; Jekeli, 2001; Vorbrich, 2003; Titterton and Weston, 2004). The most pronounced of the predictable and compensable errors are $S_{Zacc}, S_{Zgyro}, \mathbf{B}_{Zacc}, \mathbf{B}_{Zgyro}$. Random biases $\mathbf{n}_{Zacc}, \mathbf{n}_{Zgyro}$ cannot be compensated accurately.

2.1.2. General Input/Output equation of the IS and the dynamics dependence of the IS' error sources

In the "dead band" the input values, i.e. dynamics, are too low for I/O function sensitivity. "Dead band" is for example caused by the mechanical stiction, cf. (Kayton and Fried, 1997, p. 323; Allameh, 2003, pp. 4115, 4120; Zhao, 2003) and/or by thermo-mechanical white noise level (Woodman, 1997, p. 11). For Low Cost IS the "dead band" width may not be negligible (see Kayton and Fried (1997, p. 323, and passim) and section 3.2.7). In the "saturation band", the dynamics are too high for I/O (quasi-) linearity. When the I/O function is linear in the "optimum-input band" then

$$SIG_{output} \equiv K \cdot SIG_{input} + B \tag{4}$$

where SIG_{output} – output signal, SIG_{input} – input signal, and B – bias. The term K in equation (4) is called here the scale factor (of IS – valid for any accelerometer and/or any gyro generally). Therefore, in particular for Z-axis IS the three terms: K and S_{Zacc}, S_{Zgyro} are related in terms of both the physical quantity and physical property and also the three terms: B, and the magnitudes B_{Zacc} and B_{Zgyro} are related in the

above-mentioned terms. Equation (4) describes certain general and ideal case in the absence of the additional random bias terms n_{Zacc}, n_{Zgyro}. The B factor could change from warm-up to warm-up, cf. (Kayton and Fried, 1997, p. 323). For any-axis rate gyro, its bias B_{gyro} when integrated, causes an angular error, which grows linearly with time. However, for any-axis accelerometer, its bias error B_{acc}, when double integrated, causes an error in position which grows quadratically with time, cf. (Woodman, 1997, pp. 11, 15). Generally, the stability of the K factor for any IS (accelerometer or gyro) may depend on the I/O function, while specifically the stability of S_{gyro} is probably the single most important factor in the *INS* positioning accuracy deterioration with time, cf. (Kayton and Fried, 1997, p. 323). For a more detailed discussion of the above cf. (Lawrence, 1993; Jekeli, 2001; Titterton and Weston, 2004).

The following is applicable to all kinds of gyros: if a mission involves changing direction for a long time (circular routes at a rate Ω over time t), than the Z-axis gyro scale factor error $\delta S_{\varpi Z gyro}$ influences the heading error δAz in the following way: $\delta Az = \left(\delta S_{\varpi Z gyro}/S_{\varpi Z gyro}\right)\Omega t$, cf. (Lawrence, 1993, pp. 26, 27).

The contemporary specialty literature shows the growing interest in tracing of the dynamics-wise dependence of the errors of the MEMS ISs. The subject of the errors of the MEMS accelerometers and gyros in the static mode is perused in some detail by Lobontiu and Garcia (2005, pp. 267, 269, 273, and passim). The literature points to the necessity of isolating the MEMS from the vibration induced noise. For example, Bose (1996, pp. 11–17) provides some numerical examples of the influence of the vibration-induced noise on the MAG output on the angle rate error.[3] Table 1 shows for the MKII the nominal values of the bias, scale factor and their dynamical "borders".

Table 1. MKII – nominal bias, scale factor, lower border of the "saturation band" (range)

1	2	Bias (factory set)		Scale factor		Standard range			Threshold/ resolution		Full scale output	Input voltage
{g}	ł / h	acc [V]	gyro [V]	acc {V/g}	gyro {V/^{o}/s}	acc {g}	gyro {^{o}/s}	gyro {s/2π}	acc {μg}	gyro {^{o}/s}	analogue [V]	dc [V]
±1	ł	2.5	2.5	0.750	–0.027	±1.5	±75	±4.8	$\leqslant$ 10	$\leqslant$ 0.004	+4.050	+12
±3	ł	2.5	2.5	0.750	–0.027	±2.7	±75	±4.8	$\leqslant$ 10	$\leqslant$ 0.004	+4.050	+12
±1	h	0.0	0.0	–6.680	0.133	±1.5	±75	±4.8	$\leqslant$ 10	$\leqslant$ 0.004	±10	±15
±3	h	0.0	0.0	–3.330	0.133	±2.7	±75	±4.8	$\leqslant$ 10	$\leqslant$ 0.004	±10	±15

Notes: cf. (Systron Donner Inertial, 2008, pp. 13–16); column 1 – "Version Standard Range {g} Category" (see Standard range (saturation)); column 2 – mode ł/h – Mode Low/High; Full scale output for mode Low ł: 0.475 – 4.525 V; Volt. – Voltage; Input voltage: ±15 V is often cited as Standard Dual Supply (bipolar); the brackets [] signify physical units in SI and brackets {} signify non-SI physical units, in particular {g} ≡ $\tilde{n}$*(Earth)* [m/s^2], $\tilde{n}$*(Earth)* ≈ 9.80665 for the nominal "average" value at the Earth's surface, known as standard gravity; in particular {$\check{g}$} ≡ $\check{n}$*(Earth)* [m/s^2], where $\check{n}$*(Earth)* = 9.8 was adopted for the simplicity reasons.

[3] MAG – Micromachined Accelerometer Gyro.

2.1.3. Basic method for the laboratory determination of MKII accelerometer bias and scale factor

Let us adopt the equation (1b) above to a laboratory situation, assuming that the MKII ISs' analogue output in [V] is digitalised by means of the A/D card and stored on a PC.

Let us then suppose for the simplicity reasons, that Z-axis accelerometer is (within sensitivity specified by $\mathbf{n}_{Zacc}$ in (1b)) to our purposes nearly vertical and (within this sensitivity) the $\mathbf{B}_{Zacc}$ and S_{Zacc} are constant, the I/O function is symmetrical. Let the *IMU* signal be PC stored in the *IMU*'s Up and Down (Dn) positions with reference to the Z-axis accelerometer. Further let the magnitudes of

$$B_{Zacc}\,(\mathrm{Up}) = B_{Zacc}\,(\mathrm{Dn}) = B_{Zacc} \quad \text{and} \quad S_{Zacc}\,(\mathrm{Up}) = S_{Zacc}\,(\mathrm{Dn}) = S_{Zacc}$$

within three hours time span between "L" experiment commencement and "U" experiment completion (cf. Table 4).

Then the sum of the readings in [V] of the output, that is magnitudes $g_{Z_0}\,(\mathrm{Up})$, $g_{Z_0}\,(\mathrm{Dn})$ of the readings of the Z-axis accelerometer facing in sequence Up and then Down respectively, should after the relevant transformation of (1b) lead to the determination of the bias magnitude B_{Zacc} [V] as follows:

$$B_{Zacc} = [g_{Z_0}\,(\mathrm{Up}) - g_{Z_0}\,(\mathrm{Dn})]/2.0 + g_{Z_0}\,(\mathrm{Dn}) \tag{5}$$

where [V] contains the units of the accelerometer raw data digitized output in Volts.

In addition, similarly to the above, the difference between the reading in [V] of the output of the Z-axis accelerometer facing Up and Down respectively, should after the relevant transformation of (1b) lead to the determination of the scale factor magnitude $S_{Zacc}\{V/g(local)\}$

$$S_{Zacc} = \{\mathrm{mod}[g_{Z_0}\,(\mathrm{Up}) - B_{Zacc}] + \mathrm{mod}[g_{Z_0}\,(\mathrm{Dn}) - B_{Zacc}]\}/2.0 \tag{6}$$

where $g(local)$ is the magnitude of the gravity vector $\mathbf{g}(local)$, and the above coefficient 2.0 would be true if the Z axis were strictly vertical (i.e. strictly parallel to the direction of $\mathbf{g}(local)$) and so when the statement written for the magnitudes $g \approx g_Z(\mathrm{Up}) \approx g_Z(\mathrm{Dn})$ would be true.

The equations (5) and (6) were used in the calculations cited in the experimental chapter, Table 5.

2.2. The EU JRP [D]GPS/IMU(MKI) integrated system in [D]GPS/INS(MKI) mode

The EU JRP strapdown integrated system *[D]GPS/IMU*(MKI) (further called system) was conceived during the European Union Polish-German Joint Research Project (further called EU JRP). The master computer and its software together with the *DGPS*

and MKI hardware form the *[D]GPS/IMU*-AeroNav-H (or simply ANH) subsystem assembled for the EU JRP by the "AERODATA" Company in Braunschweig, Germany. The "research" software (further called *[D]GPS/IMU*-R), installed on slave-PC subordinated to ANH, has been prepared for the EU JRP by the Institute of Flight Guidance and Control at the Technical University in Braunschweig (TUBS.IFF) with the participation of the Space Research Centre of the Polish Academy of Sciences, in particular with the participation of the present author. Since its creation the system has undergone a series of maintenance and modification, cf. (Vorbrich, 2001b).

Table 2. Block diagram and configuration and description of the *[D]GPS/IMU*-R system in [*D]GPS/INS*(MKI) mode

Configuration	Description
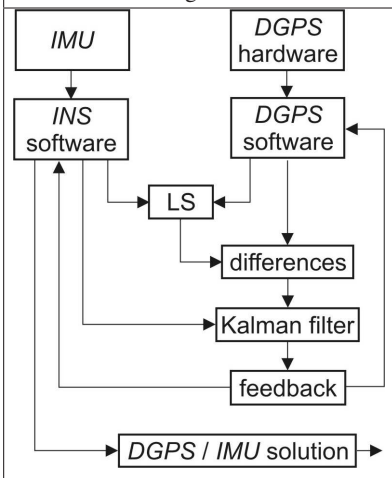	*IMU* to *INS* mechanization algorithm in [*D]GPS/INS*(MKI) mode delivers the *INS* inertial navigation solution (position, velocity and attitude). In turn the *DGPS* delivers satellite navigation solution in terms of position, velocity, pseudo--ranges and pseudorange-rates. The reference trajectory immediately fed to the Kalman filter is provided by the combined effect of the satellite and inertial position and velocity errors thought of in terms of the pseudo-range and pseudorange-rate differences (satellite-derived "observed" minus *INS*-"Least Squares calculated"). The closed loop leads to an extended Kalman filter. The system output is slaved to *GPS* time and is contained in a state vector, which for example has 17 state variables, cf. equation (7) below and in *IMU* (50 Hz) and *[D]GPS* (1 Hz) raw data matrices.

Note: see (Wagner and Wieneke, 2003, p. 544) for a block diagram of an alternative *DGPS/IMU* mode where *INS* software is omitted altogether and the raw *IMU* data and *DGPS* ranges and range rates are input to the Kalman filter. In ibid. the feedback loop shown in Table 2 is also omitted.

The Kalman filter design in the EU JRP system is flexible. For example the state vector $\mathbf{x}_{DGPS/IMU}$ in the Kalman filter mentioned in Table 2 can have 17 state variables and can be expressed as follows:

$$\mathbf{x}_{DGPS/IMU} = [\delta\,\mathbf{POS},\ \delta\,\mathbf{VEL},\ \delta\,\boldsymbol{\varepsilon},\ \delta\,\mathbf{B}_{acc},\ \delta\,\mathbf{B}_{gyro},\ \delta\,t,\ \delta\,\dot{t}\,]^{\mathrm{T}} \tag{7}$$

where there are 9 vehicle or navigation error states (that is three position states $\delta\,\mathbf{POS}$, three velocity states $\delta\,\mathbf{VEL}$, and three attitude (Euler angles) error states $\delta\boldsymbol{\varepsilon}$ (where the heading orientation error is the most important one for waterborne or landborne navigation), 6 *IMU* sensor error states (3 corrections to predetermined accelerometer biases forming $\delta\,\mathbf{B}_{acc}$ sub-vector and 3 corrections to predetermined gyro- biases forming $\delta\,\mathbf{B}_{gyro}$ sub-vector), 2 *GPS* receiver states (*GPS* clock error δt and *GPS* clock drift $\delta\,\dot{t}$). In one of its designs the Kalman filter in Table 2 can track in time domain the gyro drifting $\delta\,\mathbf{D}_{gyro}$ which is one of the key elements of such a filter design.

Also, cf. comparable solution in: (Wagner and Wieneke, 2003, p. 546) where 18 state variables state vector is very similar to (7), it solves for four quaternions instead of for three Euler angles, however.

For modern solution comparable to this presented in Table 2 see (Abdel-Hamid et al., 2006, p. 3). Also the similar method of calculating of the pseudorange and pseudorange-rate differences needed for the satellite – inertial o – c differences input into the extended Kalman filter (shown in Table 2) present (Wagner and Wieneke, 2003, p. 544; Kreye et al., 2005, p. 106, and passim). On the other hand Wagner and Wieneke (2003, p. 543, and passim) propose also serious modification of the above-mentioned method, albeit all based on (7) and Kalman filtering, cf. (Wagner and Wieneke, 2003, pp. 544, 546, and passim) and cf. Note to Table 2. According to Wagner and Wieneke (2003, p. 549) this new method which is working in the pure *DGPS/IMU*(MotionPak) mode instead of the *DGPS/INS*(MKI) mode proposed by the present paper, is not expected to improve the navigation solution accuracy during the standard dynamics of movement. However, it should slightly or moderately improve the system estimation quality during the very small dynamics of movement.

Modern literature sometimes proposes that the integrated satellite/Low-Cost *IMU* system based on the Kalman filtering for some applications could be replaced or aided by the other mathematical solutions such as the Multi-layer Feed-forward Neural Networks (MFNN), the Constructive Neural Network (CNN) (Huang and Chiang, 2008), the Artificial Neural Network (Kaygýsýz et al., 2007), and the Fussy Modelling (Abdel-Hamid et al., 2006, p. 3). Nevertheless, Wagner and Wieneke (2003, p. 544) point out that the conventional methods based on Kalman filtering and similar to the one shown in Table 2 are widely accepted.

The direct indication of the accuracy of the state vector (7) estimate is given by the diagonal elements of the state covariance matrix $\mathbf{C_x}(+)$ for the optimal estimate. Equations modelling the error propagation within the Kalman-filter-integrated *DGPS/IMU* system are given in more detail in (Vorbrich, 2001a).

The state vector in Kalman filter expressed by (7) describes one of the simplest possible cases of the inertial sensor's errors determination. Clearly, Kalman filter state vector, which has 17 state variables described by (7) does not include information on the accelerometer and gyro scale factor, and gyro drifts. Prior to the mobile experiments, these last mentioned MKI's parameters, together with the previously mentioned accelerometer biases and gyro-drift rates, were determined at the AERODATA's laboratory both during the EU JRP and during the later modifications done within the framework of the Project financially supported by the Polish Committee for Scientific Research.

Inertial literature advocates elimination of the vertical channel from the surface waterborne and level landborne satellite/inertial solution, cf. (Chatfield, 1997, p. 13). It is due to the positive feedback of the altitude errors through the gravity model. It makes *INS*'s solution unstable for the vertical channel.

2.3. The observability of the [D]GPS/IMU and [D]GPS/INS

According to Wagner and Wieneke (2003, p. 547) who cited (Dambeck, 1995) the problem described by equation type (7) is weakly observable. The predicament connected with the observability of the *[D]GPS/IMU* and/or *[D]GPS/INS* has been described extensively by the modern inertial literature. Also the sensitivity of the said observability to the dynamics of movement of the platform bearing the *[D]GPS/IMU* and/or *[D]GPS/INS* has been well known and dealt in detail by this literature.

In particular, in the observation matrix expressed in the body system of coordinates the elements for the rows $\delta\,\boldsymbol{\varepsilon}$ and $\delta\,\mathbf{B}_{gyro}$ (cf. (7)) are each governed by the product of the vector components from the angular rate vector and the lever arm vector $\mathbf{L}$ (the last vector defines the displacement from the origin of the *IMU*'s "b" system to the *GPS* antenna electric centre). During the low dynamics of the platform's movement, the above-mentioned rows do not lead to a full matrix rank, thus the system becomes unobservable. For the exact formulae necessary for the solving of the lever arm problem in the integrated satellite/*INS* system see (Wagner and Wieneke, 2003, p. 546). According to the formulae presented in ibid., theoretically the increasing of the lever arm to the full extent of such structure as the tip of the wing of a test aircraft should decrease the problem of the system unobservability due to the dramatically decreased weakness of the state vector $\mathbf{x}_{DGPS/IMU}$ in (7) in the very low dynamics of movement. However, the present author was unable to confirm this assumption experimentally.

In general the problem of the initial determination of the sub-vectors $\delta\,\boldsymbol{\varepsilon}$ and $\mathbf{L}$ belongs to the issue of the alignment. Mun et al. (2005, pp. 1257–1262) provide the mathematical formulae and the following conclusions on the observability properties of the *GPS/IMU* alignment under different system's dynamics. If a platform experiences changes in angular velocity (moves with the angular acceleration which is not zero) with reference to a given direction, then the components of lever arm error that are perpendicular to the direction of the angular velocity become observable. Linear accelerations' changes make observable the components of the relative attitude error that were perpendicular to the direction of the acceleration change.

2.4. Initialisation/alignment of [D]GPS/(Low-Cost IMU) System

By initiation we understand here all the procedures needed after the warm-up to prepare the system for the dynamic mission. The alignment procedure itself determines the initial Euler angles for the initial transformation matrix from "b" to the computations frame. Cf. *GNSS/INS* alignment procedure and the *INS* static tests' procedure mentioned in (Kreye et al., 2005, p. 103).[4] Also cf. the alternative method proposed by Hao et al. (2008, p. 117, and passim), which for *GPS*/Low-Cost *IMU* uses Kalman filter for the coarse alignment during the static phase of several minutes duration and the

[4] *GNSS* – Global Navigation Satellite System.

H (mini-max) filter for the fine tuning of the residual misalignment angles conducted under the moderate dynamics of app. 0.1 $\{\check{g}\}$.

For *[D]GPS/*MKI alignment to take place the *[D]GPS/IMU*-R software requires the availability of an external heading sensor input, for example electronic magnetic compass, cf. (Nguyen et al., 2009, pp. 861, 864). The *[D]GPS/IMU*-R software alignment procedures normally are based on **g** as a reference (cf. eq. (1b)) and the MKII laboratory stationary tests shown by the Figures 1a, 1b, 2a, and 2c. Therefore, during the alignment, the *DGPS/IMU* host-vehicle must be brought to a complete stop and it should not vibrate. During initialisation, the alignment of the ISs in terms of the estimation of inertial sensor mean biases (by means of a Kalman filter with state vector based on eq. (7) for zero velocity) takes place. The accuracy of the stand-alone *IMU* of the *[D]GPS/IMU* in between the *[D]GPS* updates during the mobile experiment depends on the *[D]GPS/IMU* static alignment procedure accuracy.

In the *[D]GPS/IMU*-R software the subsequent more accurate estimate of the heading (equivalent to Euler azimuth Ψ angle) can be obtained on-route from *GPS*-determined-velocity (components $v_{GPS\,E}, v_{GPS\,N}$) as follows (iteratively, so-called "on-flight" alignment, cf. (Nguyen et al., 2009, p. 861)):

$$\Psi = \operatorname{atan}\left(v_{GPS\,E}/v_{GPS\,N}\right) \tag{8}$$

3. Experiments with MKII and [D]GPS/MKI

3.1. Laboratory-based analysis of stand-alone MKII output data

This section provides an example of a set of the experiments ascertaining the MKII's accelerometer and gyro response in the stationary and rotational mode.

3.1.1. The experiments' scenario

During his attachment to the Global Positioning Systems Centre at the Nanyang Technological University Singapore (NTU) the present author among-other conducted the laboratory experiments with the MKII, cf. (Vorbrich, 2002).

3.1.2. The pictorial representation of the experimental raw data

During presented MKII laboratory tests the MKII accelerometers' bias and scale factor were initially calibrated on a horizontal test-bed by means of using the Earth's gravity vector **g** as a reference, cf. (Kayton and Fried, 1997, p. 324; Titterton and Weston, 2004; Park and Gao, 2006, pp. 35, 38). All the data presented in this section below refer to the A/D card with the resolution of 24 bits, and a common warm-up time. For some information about the importance of the common warm-up time for a chain of inertial experiments see (Kayton and Fried, 1997, pp. 323, 381).

Table 3. Variable features of MKII laboratory experiments' sequence Mb24J31

Figures	Experiment's name suffix	Dynamics mode	Reference or rotation axis	A/D sample rate [Hz]
1a,1b,1c	L	stationary	*Z* facing up (Up)	10
2a,2b,2c	U	stationary	*Z* facing down (Dn)	10
3a,3b,3c,4a,4b	M	rotation	rot ACW: *Z*-Up/*Z*-Dn/ *Z*-Up via *Y* kept horizontal	100
4c	T	rotation	rot 90° CW/ 90° ACW via *Z* kept facing Up	100

Note: The ambient temperature was kept constant to within ±0.5°C.

Table 4. Stationary experiments' time span

Experiment name	L	U	Between L start and U end
Time span	820 s	app. 1000 s	app. 3 hours

3.1.2.1. The stationary experiments' (selected) drawings

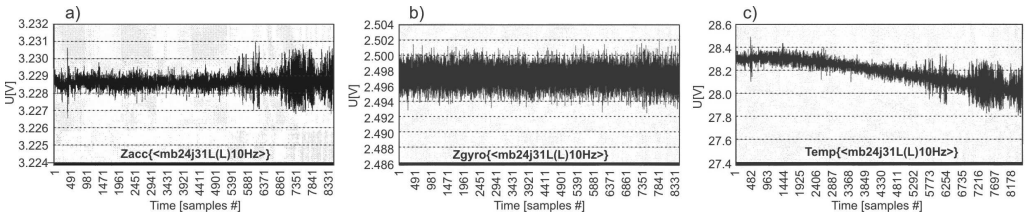

Fig. 1. *Z*-axis accelerometer experiment L a); *Z*-axis gyroscope experiment L b); MKII internal temperature experiment L c)

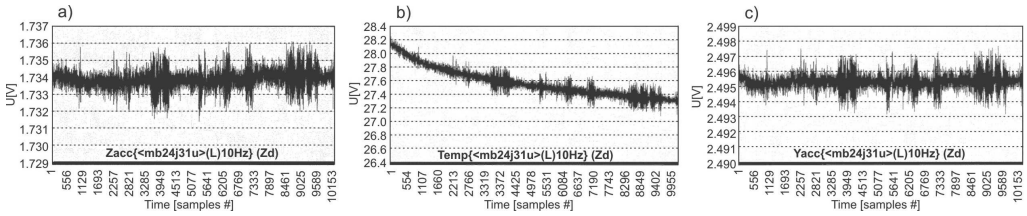

Fig. 2. *Z*-axis accelerometer experiment U a); MKII internal temperature experiment U b); *Y*-axis accelerometer experiment U c)

3.1.2.2. The rotational experiments' (selected) drawings

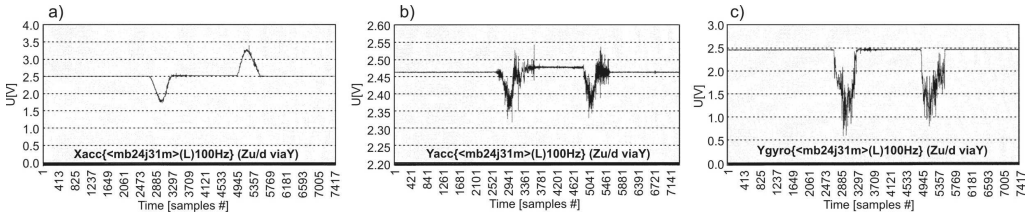

Fig. 3. *X*-axis accelerometer experiment M a); *Y*-axis accelerometer experiment M b); *Y*-axis gyroscope experiment M c)

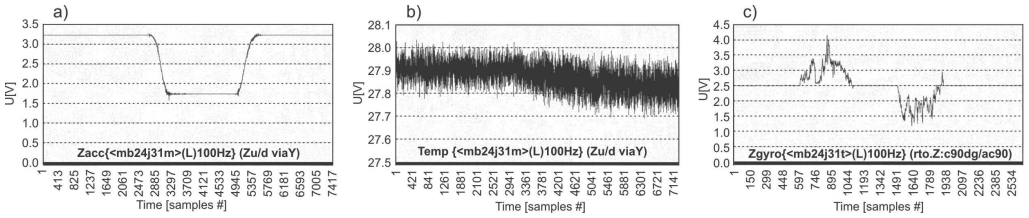

Fig. 4. *Z*-axis accelerometer experiment M a); MKII internal temperature experiment M b); *Z*-axis gyroscope experiment T c)

3.1.3. The tabularised representation of the data and the explanations

Table 5. Data for incipient determination of the bias and scale factor of the NTU MKII accelerometers

Stationary experiments L and U (see Tables 3 and 4, and family of Figures 1 and 2)			
Body "b" system axis	L (*Z* faces Up) minus U (*Z* faces Dn); mean [V]	Bias [V]	Scale factor S_{Zacc} {V/*g*(*local*)}
X(h) nearly horizontal	–0.015	–	–
Y(h) nearly horizontal	–0.017	–	–
Z(v) nearly vertical	1.495	2.481	0.745
Dynamic experiment M (see Table 3, and family of Figures 3 and Figures 4a, 4b)			
Body "b" system axes (h) – nearly horizontal (v) – nearly vertical	*Z* faces Up minus *Z* faces Dn for *Z*(v) *X* facing Up minus *X* facing Dn for *X*(v) Rotation via *Y* (ACW); mean [V]	Bias [V]	Scale factor S_{Zacc} {V/*g*(*local*)}
X(h)	0.021	–	–
Y(h)	0.016	–	–
Z(v) faces Up then Dn	1.509	2.499	0.750
X(v) facing Dn then Up	1.500	2.500	0.750

Note: cf. Table 1. In Table 5 the bias and scale factor for *Z*(v)-axis were computed by means of the equations (5) and (6) respectively; these eq. were transformed for *X*(v)-axis, however. The observed digitalized values were depicted in the families of Figures 1, 2, and 3 and Figures 4a and 4b (i.e. accelerometers,

gyroscopes and temperature). The relevant values were in error amongst other due to the uncompensated: a) Earth's rotation influence (surmising however, that MKII's output error level is too high to sense the Earth's rotation); b) errors due to nonorthogonality and misalignment of sensitivity axes; in particular non-perpendicularity (non-verticality) of the relevant Z(v)- or X(v)-axes and the non-horizontality of the X(h)- and Y(h)-axes; c) cross-axes sensitivity (here considered negligible, cf. (Park and Gao, 2006, p. 38)). The effect b) has been caused by the combined effect of the skewed X, Y, and Z axes of the "b" system, of the tilt between the "b" system and the system of coordinates defined by the MKII enclosure walls and by the non-parallelism of these walls. In particular, if the axes X(h) and Y(h) were strictly horizontal (i.e. strictly perpendicular to the local gravity vector $\mathbf{g}(local)$ direction), then the values for delta for X(h) and Y(h) should have oscillated around the zero value [V] (within the boundaries of the measurement error). The above would be true – assuming, that all the scale factors and biases are constant (within the time span of the experiment). The actual measurement for Z(v) was long-term-static and for X(v) was dynamic. In contrast, during the actual measurement used for computation of data illustrating dynamic experiment M, the values X(h) and Y(h) were static only.

3.1.4. Determining the direction of the rotation

The "senses" of the gyration vector in (3)-like equation can be determined by means of comparison of the Figures 3a, 3b, 3c, and 4a (accelerometers and gyros) and the Figure 4c (gyro). It shows that a) ACW rotation lowers the magnitude of the output voltage of the gyros for Z-and Y-axes; b) the above mentioned fact # a) allows to control the history of the direction of the rotation (ACW versus the reverse); c) it follows that the MKII's body "b" horizontal X, Y system of axes is left-handed. In other words when the MKII is rotated ACW 90° in the X, Y plane about Z-axis, then after the 90° rotation had been completed the X-axis coincided with the previous direction and pointing (i.e. sense or arrow) of the Y-axis.

3.2. Comparative GPS, DGPS and [D]GPS/IMU solution error analysis

3.2.1. The test lake and the test-boat

Fig. 5. Lukomie (Charzykowskie) lake and some experiments' traces traversed by M/B Bartek between the unmooring and mooring event (for red trace cf. Figure 7, for violet-pink trace cf. Figure 12) and M/B Bartek

3.2.2. *DGPS/IMU* hardware mount on board the research M/B Bartek on Lukomie lake and on the jetty

M/B Bartek was built in the Ustka Shipyard and has a "Conrad 900" type of hull. It is a hybrid Diesel/electric powered research boat dedicated for the biological and zoological exploration of the Lukomie lake. The small jitter of the electric engines was important for the *[D]GPS*/MKI experiments scheduled for the very low dynamics sailing (see below). The *[D]GPS/IMU* system itself was mounted in the forward-cabin, the *GPS* antenna on top of the cabin roof (Fig. 5), and the *DGPS* reference station RS telemetry antenna mast was fixed at the Lukomie lake's jetty of the Ecological/Biological Research Centre at Funka.

Table 6. The dynamics parameters of M/B Bartek powered by the Diesel engine

Maximum speed v_{max}		Mean acceleration from 0 {knots} to v_{max}			Mean deceleration from v_{max} to 0.5 {knots}			Circulation minimal diameter at 25 {knots}	
{knots}	{km/h}	Δt [s]	(+)a [m/s^2]	{$a/\check{g}$}	Δt [s]	(-)a [m/s^2]	{$a/\check{g}$}	CW [m]	ACW [m]
26	48.15	14	3.44	0.35	120	0.21	0.02	15 app.	20 app.

Note: experimentally determined by the present author as a mean from several runs in calm weather at 0 {^{o}B}; 1 {knot} ≡ 1852 {m per hour} ≡ {Nautical Mile per hour}; {km/h} – {km per hour}; v – boat's speed relative to water, Δt – mean time span; $a = \Delta v/\Delta t$.

3.2.3. *DGPS/IMU* hardware mount on board the research M/B Imoros in the Wladyslawowo harbour

The paper also presents the *[D]GPS/*MKI experiments on board the research M/B Imoros (powered by the Diesel engines only) in the Wladyslawowo harbour. M/B Imoros and M/B Bartek have comparable dynamics characteristics, cf. (Vorbrich, 2001a).

3.2.4. *DGPS/IMU* hardware mount on board the research van

The *DGPS/*MKI-research-van was the present author's main platform, cf. (Vorbrich, 2001a). It offered easiest way to control both the reference route and the dynamics of movement.

3.2.5. Alignment/mount of *DGPS*/(Low-Cost *IMU*) System

In the stationary vehicle/boat environment (no wind, no waves, no traffic, engine not running) the optimal value of the alignment time of the *DGPS*/MKI system was found to be equal to app. 5 min. This period is consistent with the period of at least few minutes reported by the modern literature. However, Nguyen et al. (2009, p. 864) report the successful static alignment period as short as 10 s.

3.2.6. Comparative *GPS*, *DGPS* and *DGPS/IMU* solution error analysis during medium to high dynamics of movement on water and on land

The methodology of the tests described below in the paper to a considerable extent agrees with the comparable satellite/Low-Cost *IMU* tests described in the contemporary literature, in particular cf. (Abdel-Hamid et al., 2006, p. 7, and passim; Kaygýsýz et al., 2007, p. 175; Huang and Chiang, 2008, p. 140, and passim; Nguyen et al., 2009, p. 866). Also see the comparable airborne satellite/MotionPak test methodology in: (Wagner and Wieneke, 2003, p. 547, and passim).

3.2.6.1. Calibrating on water the system's on-flight initialisation and alignment

The experiment 13aa reported in this paper involved: purposefully-incorrect *GPS/IMU* "stop" phase initialisation and alignment followed by incorrect *GPS/IMU* on-flight alignment during low-dynamics movement further followed by successful *GPS/IMU* on-flight alignment during high-dynamics circulation.

To avoid the anticipated problems with the intermittent telemetry outage and its impact on the Kalman filter, the RS telemetry transmitter was turned off completely.

In Figure 6, apart of the initial erratic manoeuvres discernible at the bottom right-hand-side-corner of the latitude/longitude LAT/LON trace; there are visible three distinctive legs: 1) outward, good visibility facilitated semi-straight course app. NWbW, the sole-*GPS* solution is smooth and can serve as a reference, while the *GPS/IMU*

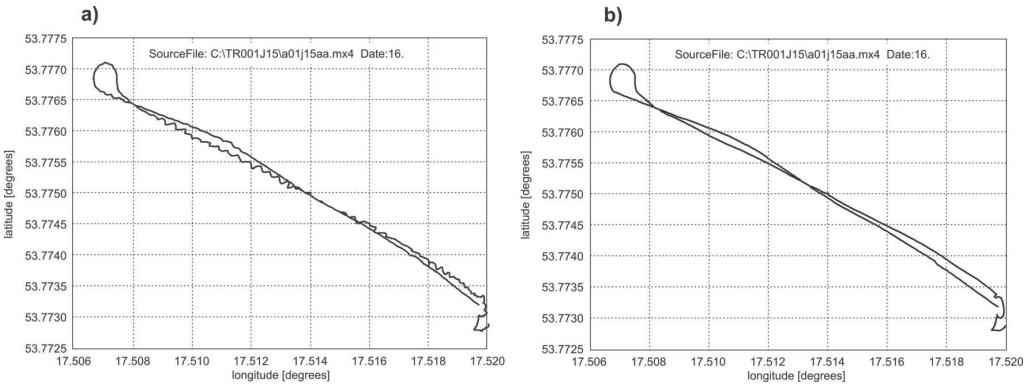

Fig. 6. Experiment 15aa LAT/LON *GPS/*MKI solution a); and LAT/LON sole-*GPS* solution b)

solution, following the "stop phase's" incorrect initialisation and alignment, did not converge, was wavy, not smooth; the straight-course-low-dynamics on-flight alignment is not effective; 2) high dynamics circulation 270° CW plus 90° ACW at the upper left-hand-side-corner of the drawing; 3) return leg, course app. SE to SEbE when the *GPS/IMU* solution is smooth following the correct on-flight alignment effected by the high dynamics circulation mentioned in point 2) above.

Table 7. Experiment 15aa *GPS/IMU* on-flight alignment following the deliberately erroneous "stop phase" alignment

#	Phase	t\{h:min\} or Δt {min}	Notes	System	σ [m]
1	stop	$\Delta t \approx 2$	Diesel engine on, moored boat rolling on waves (wash)	(I+A)	±10
2	OFA	17:11	**low-**dynamics manoeuvres nearby the Funka jetty	NOK	±10
3	out OFA	$\Delta t \approx 6$	**low-**dynamics semi-straight course app. NW, at 17:12 velocity *GPS* – 6.1 knots, wind app. S, steady 2-3 {°B}	NOK	±7
4	OFA	17:17	**high-**dynamics tight circulation 270° CW + 90° ACW	OK	–
5	return	$\Delta t \approx 8$	**low-**dynamics semi-straight course app. SE	OK	±7
6	mooring	17:26	mobile experiment duration: 17:11 – 17:26, Δt = 15 min	OK	±7

Note: sailing mission powered by Diesel; t – time; Δt – phase duration; {h:min} – {hour:minute *GPS* time local zone}; (I+A) – "stop phase" initiation and alignment; OFA – on-flight alignment; system – system state; NOK – *GPS*/MKI Kalman filter LAT/LON solution not converging; OK – successful OFA and Kalman filter LAT/LON convergence; after the tight circular movement (# 4) had been completed, the alignment oscillations definitely ceased, oscillations in the LAT/LON navigation solution *GPS*/MKI was smooth (# 5); σ – Sig POS from Kalman filter variance/covariance matrix.

3.2.6.2. GPS signal outage problems in the sole-GPS solution smoothed by the integrated DGPS/MKI solution during high dynamics rotation on the lake

Cf. Figure 5 (left-hand-side-apex of the red trace) and Figure 7. After the correct system initialisation the boat was cruising at full speed app. WNW-half-W course. Then at the apex of this course, the helm was put hard left and the boat turned almost instantly app. 180°. During this rotation, the signal from some of the satellites was blocked by the nearby woods and the *IMU* was operating in the stand-alone mode. Then the boat resumed her app. ESE-half-E course. Integrated *DGPS*/*IMU* solution serves as a reference for studying the the short-term stand-alone *IMU* solution.

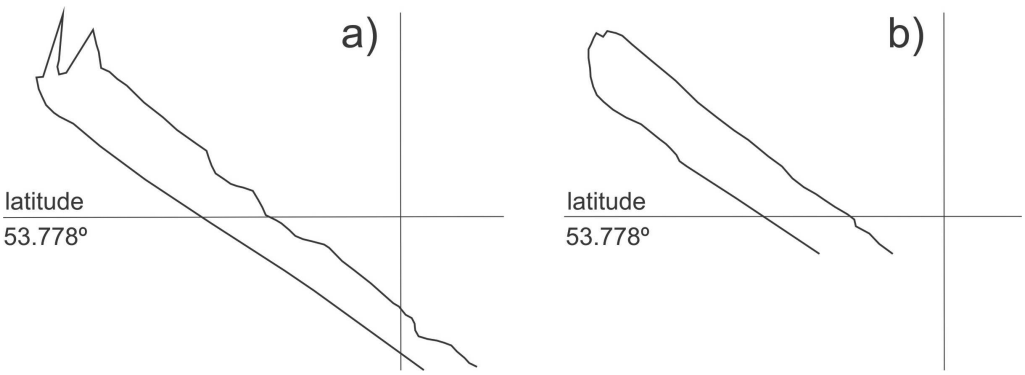

Fig. 7. Sole-*GPS* a); *DGPS*/MKI b)

Note: According to the manufacturer the CEP – Circular Error Probable of a very well tuned MotionPak I *IMU* in a stand-alone mode roving with the rather high dynamics below the saturation band level of the I/O function obeys the following equation: CEP[m] = SQRT $[k_0^2 + (k_2\Delta t^2)^2 + (k_3\Delta t^3)^2]$; where k_2 <app. $1\cdot10^{-2}$; k_3 < app. $1\cdot10^{-4}$ where the constants k_0 [m], k_2 [m/s^2], and k_3 [m/s^3] were given by the manufacturer as approximate 1 σ (one sigma) values.

3.2.6.3. GPS signal outage problems in the stand-alone DGPS solution smoothed by the integrated DGPS/MKI solution during average waterborne dynamics movement in the Wladyslawowo harbour

As mentioned in section 3.2.3, the *DGPS/*MKI mobile experiments were conducted on board M/B Imoros in Wladyslawowo (*DGPS* RS at Rozewie lighthouse). The boat sailed in the vicinity of water-walls and jetties so the sailing path was controlled within a metre. *DGPS/*MKI system retained the ±1 m to ±2 m one sigma (Kalman filter) accuracy and effectively bridged *DGPS* solution LAT/LON gaps caused by the satellite signal shadowing and multipath (Figures 8a and 8b). The landborne reference was created by the van-*DGPS/*MKI solution. The van at night followed the details of the port (no *GPS* gaps), cf. Figure 8c.

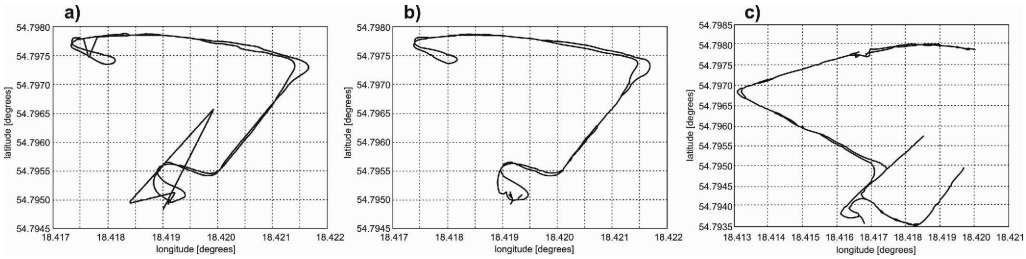

Fig. 8. WLA, water, *DGPS* solution a); WLA, water, *DGPS/*MKI b); WLA, van, *DGPS/*MKI c)

3.2.6.4. GPS signal outage problems (overhead bridge) in the stand-alone GPS solution smoothed by the GPS/MKI solution during average landborne dynamics movement proceeded by high dynamics, PRCT

Results from sample experiment when the van travelled five routes in ACW direction on the Poznan Racing Car Track PRCT – see Figure 9. The greatest dynamics of movement – 0.5 {ğ} – were experienced in the northernmost part of the track, the van first accelerating to 100 km/h and then braking rapidly with the deceleration up to 0.5 {ğ} while approaching the NE turn corner and then the overhead bridge. Figure 9a shows the sole-*GPS* solution LAT/LON positions and the gap in these solutions caused by *GPS* signal obstruction under the bridge. Figure 9b presents the uninterrupted *GPS/*MKI solution.

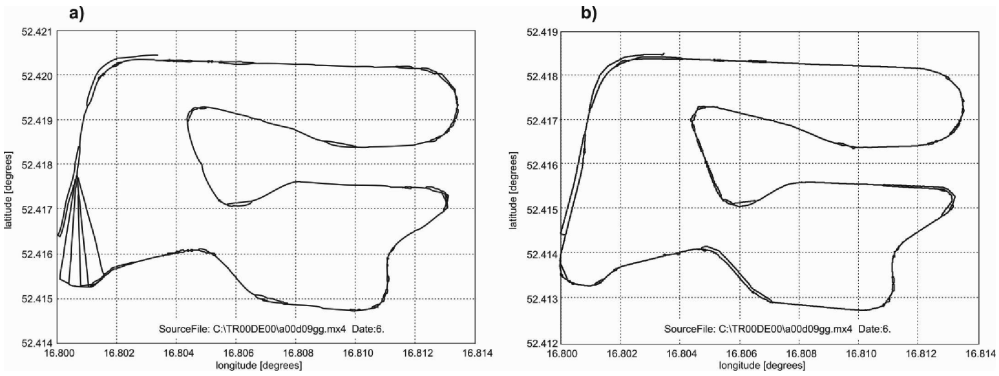

Fig. 9. PRCT, sole-*GPS,* ACW connected points, 1 Hz a); PRCT, *DGPS/*MKI, ACW, 50 Hz b)

3.2.6.5. GPS signal outage problems (buildings, lorries traffic) in the stand-alone DGPS solution smoothed by the integrated DGPS/MKI solution during average to low landborne dynamics movement

The Cracow AGH University of Science and Technology *DGPS/*MKI test-bed presents map Fig. 10a and semi-rectangle in red ink to the left. The *DGPS* RS was located at the roof of the AGH building (right). The van completed two circulations CW, no-stop, with an average speed and dynamics of movement, apart of some of the distances on the Armii Krajowej St. when both the speed and dynamics were very low due to very dense traffic. Figure 10b shows the stand-alone *DGPS* solution LAT/LON positions and the gaps in this solution caused by the *GPS* signal obstruction effected by the hotels (left) and the high-lorries passing on the Armii Krajowej St. In contrast, Figure 10c presents the completely uninterrupted *DGPS/*MKI solution. Cf. the response of the short-term stand-alone *IMU* solution of the *DGPS/IMU* to different signal outages and different dynamics of movement scenario in (Huang and Chiang, 2008, pp. 141, 143).

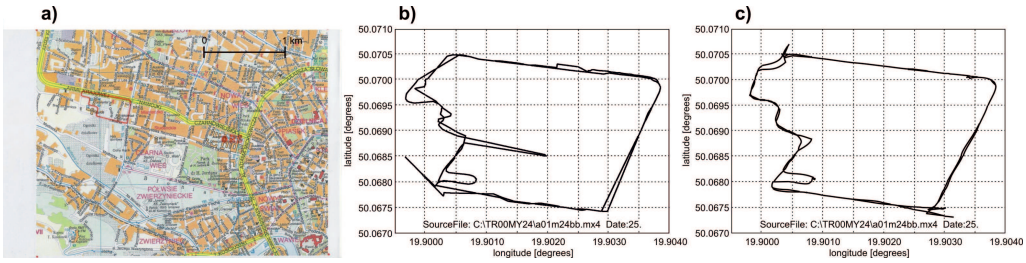

Fig. 10. Cracow AGH test-bed a); AGH stand-alone *DGPS* b); AGH *DGPS*/MKI c)

3.2.6.6. Telemetry outage problems in the stand-alone DGPS smoothed by integrated DGPS/IMU solution

Telemetry signal outage problems in the stand-alone *DGPS* solution were caused most probably by the saturation of the telemetry signal by the strong-signal military radar, mounted relatively nearby.

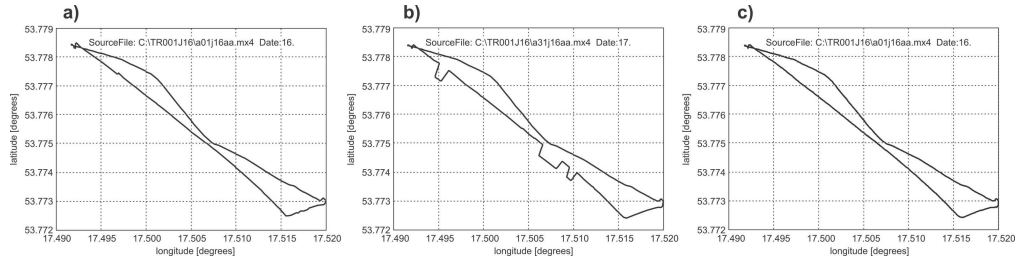

Fig. 11. Experiment 16aa; sole-*GPS* solution a); *DGPS* solution b); *DGPS/IMU* solution c)

Table 8. Experiment 16aa; main problem – stand-alone *DGPS* solution probable telemetry outage

#	Phase /leg	t {h:min} or Δt {min}	Notes	*GPS*	*DGPS*	*DGPS* /MKI	σ [m]
1	stop	$\Delta t \approx 5$	I+A OK	OK	OK	OK	±1
2	out	10:41 – 10:50/1 $\Delta t \approx 10$	Funka RS – Kopernica landing stage. Poor visibility: first 2/3 part of leg steering compass course (Kopernica not visible), last 1/3 part steering to visible Kopernica	OK	OK	OK	±1
3	turn back	10:51 $\Delta t \approx 1$	Kopernica landing stage dist. app. 10 m stop; then turn going astern portside CW 90° then forward CW 90°	OK	OK	OK	±2
4	return	10:51 – 11:01 $\Delta t \approx 10$	from #3 steering towards the objects in-line at Funka slipway (well defined and moderately visible). *DGPS* deteriorates 3 times when telemetry outage observed	OK	**NOK** outages	OK	±1
5	final appr.	11:01 – 11:02 $\Delta t \approx 2$	after approaching Funka slipway turning abruptly 90° ACW portside and steering along the Funka shore then turning sharply CW towards Funka RS and mooring	OK	OK	OK	±1
6	stop	$\Delta t \approx 5$	misclosure comp.; mobile exp. duration: $\Delta t \approx 21$ min	OK	OK	OK	±1

Note: Diesel engine; t, Δt, (I+A) and σ – see Note to Table 7; meteo: wind S, 2–3 {°B}, water 3 {°P}, visibility phase # 2 bad to poor, #4 moderate; {°P} – Petersen scale.[5]

3.2.7. Deterioration of the DGPS/IMU solution with reference to the DGPS solution and the GPS solution during extremely low dynamics of movement on water

The experiment time-wise description: at first the boat was sailing under her electric engine app. NWbN pilot course (cf. Figure 5, violet-pink trace). Then at the apex of this cruising the engine was stopped and the boat was drifting (see upper part of the drawings LAT/LON in Figure 12). Then the electric engine was started and engaged again and the boat sailed first app. SW and then finally took app. SE course back to her moorings. During the drift phase, the stand-alone *DGPS* solution serves as a reference for studying the *IMU* accelerometers' behaviour in the case when both the linear accelerations and turn-rates are so low as to approach the "dead-band" of the *IMU* I/O function.

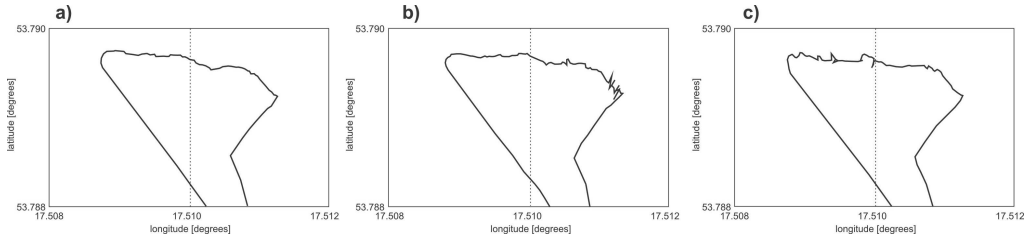

Fig. 12. Stand-alone *DGPS* solution a); *DGPS*/MKI solution b); sole-*GPS* solution c)

Table 9. Computational Conclusions Lake-Borne *[D]GPS/IMU* – Drift. Voyage # 01J15cc

Boundaries/conditions				
Drift time span {min}	Wind direction and {°B}	Lake – water {°P}	Drift speed over water {knots}	Drift speed over bottom {knots}
19:16 to 19:47, $\Delta t \approx 31$	West 1÷2	2	0.25	0.25
Accuracy one sigma [m] POS from Kalman filter variance/covariance matrix during the drift phase				
Drift time span {min}	stand-alone *DGPS* σ [m]		*[D]GPS/IMU* σ [m]	sole-GPS σ [m]
31	±2		±2 to ±8	±6 to ±10

Note: electric engine in transit, during the drift phase engine stopped, cf. Figure 12.

[5] In 1927 P. Petersen, a German sea captain, published a scale from 0 to 12 for the state-of-the-sea.

4. Conclusions

4.1. The conclusions from the MKII laboratory experiments

Table 5 shows that the values of the MKII accelerometer bias and scale factors determined separately during long-term (3 hours) stationary tests and separately during rotation are remarkably comparable for the Z-axis and X-axis and comparable to the specification provided by Table 1. Figures 1 to 4a show that under constant laboratory conditions the inertial and gravitational specific forces could well be separated phenomenologically. Therefore, according to both above worded conclusions the gravity **g** calibrated MKII accelerometer well. This in turn could be utilized during the *[D]GPS/IMU* field experiments combining the forces according to (1c)-like and (2)-like equations.

The laboratory experiments in general confirmed the assertions of the inertial literature of the necessity of maintaining the MKII's internal temperature reasonably constant. Nevertheless, the cross-correlation in time domain between the MKII internal temperature output and gyro output was negligible, cf. Figures 1b and 1c. Interestingly, in the marked contrast the cross-correlation in time domain between the internal temperature output and the accelerometer output was notably high. However, the accelerometer's bias and scale factor computed from various experiments and axes with the common warm-up time were reasonably constant when the ambient temperature was kept constant to within ±0.5°C.

In addition, the interpretation of Figures 3 and 4 for the accelerometer and gyro shows that the MKII accelerometers can (albeit not directly) provide valuable pieces of information (in terms of direction, sense and turn rate) about the rotation vector $\bar{\omega}$ of the "body" system of coordinates with reference to the local vertical. These tests comply with the latest trends to seek accelerometer's design measuring also rotations or a gyro measuring acceleration as well, cf. (O'Brien et al., 1995, p. 9, and passim; Kayton and Fried, 1997, p. 323; Titterton and Weston, 2004, p. 153, and passim).

*4.2. The conclusions from the [D]GPS/***MKI** *lake-borne and land-borne experiments*

In the absence of the S/A the short-term telemetry outages (not coupled with the *GPS* signal outages), which by their nature did not degrade *[D]GPS/*MKI solution to the clear case sole-*GPS/*MKI nor to the stand-alone MKI, were smoothed satisfactorily by *[D]GPS/*MKI solution which uninterruptedly maintained $\sigma = \pm 1$ m accuracy during relatively low dynamics of movement on water, see Figure 11.[6]

[6] S/A – Selective Availability, off, cf. tests with the S/A-on (Vorbrich, 2001a, 2001b).

However, according to the theory, overall the performance of the *[D]GPS/*MKI system under certain conditions should depend on the dynamics of motion. It seems that none of the waterborne and landborne tests was conducted by the author with the dynamics of movement, where the MKI I/O function passed into the "saturation band". On the contrary, very high dynamics of waterborne manoeuvres in tight circulation were necessary for the successful on-flight *GPS/*MKI alignment following purposefully incorrect *GPS*/MKI "stop phase" initialisation and alignment (cf. Fig. 6a and Fig. 6b). Also, boat's tight and speedy circulation facilitated the smoothing out of the *GPS* signal outages, which led to the short-term stand-alone *IMU* MKI mode of navigation (cf. Fig. 7a and Fig. 7b).

Likewise the van's maximum achievable dynamics of motions realised by the crush braking (app. 0.5 $\{\check{g}\}$) and by the van's centrifugal accelerations in bends, facilitated the short-time calibration of the MKI's errors by means of the *DGPS*/MKI system. This in turn enhanced the short-time stand-alone MKI performance during consequent driving under the bridge with the average dynamics – Figures 9a and 9b. This kind of examination relating the *IMU* output signal to the input (in terms of the maximum and minimum linear/angular accelerations which the *INS* calibrated by *[D]/GPS/IMU* can resolve) is consistent with the investigation trends reported by the inertial literature, cf. (Titterton and Weston, 2004, pp. 264, 266, and passim). However, the procedures demonstrated in the present paper are expected to be applicable in situations where body rates may approach the MKI's sensor maximum angular rate capability only transiently. Nevertheless, the inertial literature suggests that in many applications where high turn rates coupled with the high amplitude vibrations are likely to be sustained, the procedure described in the present paper may not be adequate for the Low Cost *IMU*, cf. (Kayton and Fried, 1997, p. 324). According to the literature the *IMU* should be scaled to sense/pick up considerably more than the maximum expected short-time acceleration, in order to prevent saturation in the presence of the sustained acceleration combined with vibration, cf. ibid. Nevertheless, the inertial literature proposes that then the Low-Cost *IMU* performance should be compared for example with the ring laser gyro, which offers superior dynamic stability, cf. (Titterton and Weston, 2004).

Still, for the present author it has been impossible to ascertain the lowest applicable borders of the horizontal dynamics movement. We are writing here about the dynamic conditions, which are too low for the correct performance of the MKI during the short-term forced stand-alone mode (short term satellite signal outage). MKI in this mode performed satisfactorily during the average/low dynamics movement in the harbour when sometimes the *GPS* was cut off (Figures 8a and 8b). Likewise MKI in this mode bridged *GPS* signal outages during experiment when the van was driven slowly and jerkily along the quasi-jammed road while the *GPS* antenna was sometimes sheltered by passing lorries (Figures 10b and 10c). Similarly the *DGPS*/MKI system's solution in general mirrored closely the true pass when the van was driven comparatively slowly and jerkingly in order to follow all the details of the Wladyslawowo harbour and its jetties, cf. Figure 8c.

On the other hand, extremely low dynamics of the boat's progress over the bottom degraded to a great extend the performance of the *DGPS*/MKI with reference to the stand-alone *DGPS* solution. Summary of *IMU* MKI error testing by means of the comparison of the results of the *DGPS* and *DGPS*/MKI solutions for the drift phase (set of Figures 12a – 12c) is as follows: a) LAT/LON solutions for *DGPS* are evidently smoother than for the *DGPS*/MKI; b) During the drift phase the accuracy sigma of the 2D position for *DGPS* is on average up to four times better than for the *DGPS*/MKI; c) The above mentioned superior performance of the stand-alone *DGPS* solution with reference to the *DGPS*/MKI solution has been most probably caused by the MKI accelerometers measuring in the "dead-band" of the I/O function.

The key issue is that in the "dead-band" the "not-white-noise" and not-realistic signals of the *IMU* were wrongly interpreted by the Kalman filter, which did not converge fully satisfactorily. Wagner and Wieneke (2003, p. 548) reported comparable results of the satellite/MotionPak airborne tests. According to ibid., because of the weak satellite/MotionPak observability during platform's very low dynamics, the error variance (of the state vector equation equivalent to eq. (7) above) rises. In turn this could lead to stability problems making worthless the Kalman solution for state vector type (7).

Acknowledgments

The paper presents part of the research project code-number NN526212634, financed by the Ministry of Science and Higher Education of Poland, conducted at the Space Research Centre in Warsaw, Poland. The present author is indebted to Prof. Janusz B. Zieliński for his incessant advice concerning the subject matter of the paper.

References

Abdel-Hamid W., Abdelazim T., El-Sheimy N., Lachapelle G., (2006): *Improvement of MEMS-IMU/GPS performance using fuzzy modelling,* GPS Solutions, No 10, pp. 1-11.

Allameh S.M., (2003): *An introduction to mechanical-properties-related issues in MEMS structures,* Journal of Materials Science, No 38, pp. 4115-4123.

AAS (American Astronautical Society), (2005): *Spaceflight mechanics*, Proceedings of the AAS/AIAA: Spaceflight Mechanics Meeting, Univelt, pp. 343-344.

Bose S.C., (1996): *Solid State Sensors*, Lecture Notes on Integrated Navigation Systems (INS/GPS), Technalytics, Canoga Park, CA, USA, pp. 11-17.

Caccia M., Bibuli M., Bono R., Bruzzone G., (2008): *Basic navigation, guidance and control of an Unmanned Surface Vehicle*, Jour. Auton. Robot., Vol. 25, pp. 349-365.

Chatfield A.B., (1997): *Fundamentals of High Accuracy Inertial Navigation*: Progress in Astronautics and Aeronautics, American Institute of Astronautics and Aeronautics, 339 pp.

Dambeck J.H., (1995): *Observability and controllability analysis for a strapdown inertial navigation system*, in: K. Linkwitz, U. Hangleiter (Eds), High precision navigation 95, F.D. Ummler, Bonn, Germany, pp. 149-158.

Everett H.R., (1995): *Sensors for mobile robots: theory and application*, A.K. Peters; 528 pp.

Fontaine B., Termont D., Steinicke L., Pollefeys M., Vergauwen M., Moreas R., Xu F., Landzettel K., Steinmetz M., Brunner B., Michaelis H., Behnke T., Dequeker R., Degezelle P., Bertrand R., Visentin G., (2009): *Autonomous Operations of a Micro-Rover for Geo-Science on Mars*, PDF file published by NASA on www, Febr., 8 pp.

Grejner-Brzezinska D., (2005): *On improving navigation accuracy of GPS/INS systems*, Photogrammetric Engineering and Remote Sensing, Vol. 71, Issue 4, April 2005, pp. 377-389.

Hao Yan-ling, Chen Ming-hui, Li Liang-jun, Xu Bo, (2008): *Comparison of robust H_ filter and Kalman filter for initial alignment of inertial navigation system,* J. Marine Science & Application, Vol. 7, No 2, pp. 116-121.

Huang Yun-Wen, Chiang Kai-Wei, (2008): *An intelligent and autonomous MEMS IMU/GPS integration scheme for low cost land navigation applications,* GPS Solutions, No 12, pp, 135-146.

Jekeli Ch., (2001): *Inertial navigation systems with geodetic applications*, Walter de Gruyter, Berlin, New York, 352 pp.

Kaygýsýz B.H., Erkmen A.M., Erkmen ÿI., (2007): *Enhancing positioning accuracy of GPS/INS system during GPS outages utilizing artificial neural network,* Neural Processing Letters, No 25, pp. 171-186.

Kayton M., Fried W.R., (1997): *Avionics Navigation Systems*, Second Ed., Wiley-IEEE, 773 pp.

Kreye Ch., Hein G.W., Zimmermann B., (2005): *Evaluation of Airborne Gravimetry Integrating GNSS and Strapdown INS Observations,* Proc. IAG Symposia, Vol. 129, Geoid and Space Missions, Session 2, pp. 101-106.

Lawrence A., (1993): *Modern Inertial Technology. Navigation, Guidance & Control*, Springer-Verlag, NY, 235 pp.

Lobontiu N., Garcia E., (2005): *Mechanics of Microelectromechanical Systems*, Springer, New York, 406 pp.

Lee Mun Ki, Hong Sinpyo, Lee Man Hyung, Kwon Sun-Hong, Chun Ho-Hwan, (2005): *Observability Analysis of Alignment Errors in GPS/INS*, J. of Mechanical Science and Technology, Vol. 19, No 6, pp. 1253-1267.

Nguyen Ho Quoc Phuong, Kang Hee-Jun, Suh Young-Soo, Ro Young-Shick, (2009): *INS/GPS Integration System with DCM Based Orientation Measurement*, Lecture Notes in Computer Science, Vol. 5754, Emerging Intelligent Computing Technology and Applications, pp. 856-869.

Novara M., (2001): *The BepiColombo Mercury surface element*, Planetary and Space Science, Elsevier Science Ltd., No 49, pp. 1421-1435.

O'Brien B.B., Burns B.E., Geen J.A., (1995): *Micromachined Accelerometer Gyroscope*, US Patent No 5,392,650, 17 pp.

Park M., Gao Y., (2006): *Error Analysis and Stochastic Modelling of Low-cost MEMS Accelerometer*, Journal Intell. Robot. Syst., No 46, pp. 27-41.

Reze M., Hammond J., (2005): *Low g Inertial Sensor Based on High Aspect Ratio MEMS,* in: J. Valldorf, W. Gessner (Eds), Advanced Microsystems for Automotive Applications 2005, VDI-Buch, Springer-Verlag, Berlin, Heidelberg, New York, pp. 459-471.

Systron Donner Inertial, (2008): *MotionPak II User's Guide. # 964015, Rev E*, Systron Donner Inertial, Concord, CA, USA, 28 pp.

Teisseyre R., Minoru Takeo, Majewski E., (Eds), (2006): *Earthquake source asymmetry, structural media and rotation effects*, Springer, 582 pp.

Titterton D.H., Weston J.L., (2004): *Strapdown Inertial Navigation Technology*, IET, 558 pp.

Valldorf J., Gessner W., (2005): *Advanced Microsystems for Automotive Applications*, Springer, 543 pp.

Vorbrich K.K., (2001a): *Contribution to Vehicular, Waterborne and Airborne Navigation by Means of the DGPS/(Low-Cost IMU) Integrated System*, Artificial Satellites, Journal of Planetary Geodesy, 2000, Vol. 35, No 3, pp. 85-168.

Vorbrich K.K., (2001b): *Contribution to Vehicular Navigation and Real-Time Positioning by Means of the DGPS/(Low-Cost IMU) Integrated System,* Proc. of the 3rd International Conference on Information, Communications and Signal Processing (ICICS 2001), Singapore, 15 – 18 October 2001, pp. 5, paper nr. 0551.

Vorbrich K.K., (2002): *Integrated Satellite Navigation System. Theory, Experiments, and Applications*, Global Positioning Systems Centre, Nanyang Technological University, Singapore, 302 pp.

Vorbrich K.K., (2003): *Error Propagation in the Integrated Global Navigation Satellite System GNSS/IMU*, Proc. International Scientific/Technical Conference Engineering of the Sea-Going Traffic, Swinoujscie, Poland, 20 – 21 November 2003, Maritime Academy in Szczecin, Szczecin, Poland, pp. 261-273.

Wagner J.F., Wieneke T., (2003): *Integrating satellite and inertial navigation — conventional and new fusion approaches*, J. Control Engineering Practice, No 11, pp. 543-550.

Wang H.H., (1996): *Experiments in intervention autonomous underwater vehicles*, Stanford University, 2 Editions, OCLC # 37752534, 446 pp.

Woodman O.J., (1997): *An Introduction to Inertial Navigation,* Technical Report, No 696, UCAM-CL--TR-696, University of Cambridge Computer Laboratory, ISSN 1476-2986, 37 pp.

Zhao Y., (2003): *Stiction and Anti-Stiction in MEMS and NEMS*, Acta Mechanica Sinica (English Series), Vol. 19, No l, February, ISSN 0567-7718, pp. 1-10.

Analiza pewnych błędów „mało dokładnej" inercjalnej jednostki pomiarowej przy niskiej i wysokiej dynamice ruchu

Krzysztof K. Vorbrich

Obserwatorium Astrogeodynamiczne
Centrum Badań Kosmicznych Polskiej Akademii Nauk
Borowiec, ul. Drapałka 4, 62-035 Kórnik
e-mail: vorb@cbk.poznan.pl

Streszczenie

Część zasadnicza pracy przedstawia pewne rezultaty doświadczeń przeprowadzanych w laboratorium Uniwersytetu w Singapore i wyznaczających błędy stosunkowo „mało-dokładnej" (ag. Low-Cost lub „Low-Grade") inercjalnej jednostki pomiarowej MotionPak^{TM} typu MKII w modzie statycznym i dynamicznym. Ten ostatni był ograniczony do obrotów wokół osi poziomych układu współrzędnych wyznaczanych przez obudowę MKII. Współczynnik skali i stałe przesunięcie skalowane były wartością wektora przyspieszenia ziemskiego.

Testy polowe przeprowadzano na pokładzie statków badawczych na jeziorze i na morzu we Władysławowie oraz na lądzie na samochodzie. Praca prezentuje niektóre wyniki testów mobilnych (porównanie ciągłości rozwiązań *GPS*, *DGPS*, *DGPS*/MKI), m.in. przy dużej, średniej oraz bardzo małej (dryf statku) dynamice ruchu. Oprogramowanie umożliwiało pracę jednocześnie w modach o notacji: *[D]GPS*/MKI oraz *[D]GPS*/INS(MKI). Dla pierwszego z tych modów filtr Kalmana wykorzystywał surowe dane dla inercjalnych przyspieszeń i kątów Eulera. Dla drugiego z tych modów do filtra Kalmana wprowadzano inercjalne pseudoodległości i ich zmiany w czasie. Praca prezentuje rezultaty rozwiązania dla modu drugiego. Rozwiązanie ruchu dla *GPS, DGPS*, oraz *[D]GPS*/INS(MKI) służyło jako wzorzec dla badania ciągłości rozwiązania samo-stojącego MKI w czasie nieciągłości odbioru sygnału satelity lub telemetrii. Dodatkowo, testy wykonane na jeziorze przy prawie zerowej dynamice ruchu wykazały zmniejszenie dokładności rozwiązania *[D]GPS*/INS(MKI) w porównaniu do rozwiązania *DGPS*. Doświadczenia polowe miały m.in. na celu wykazanie prawidłowości działania oprogramowania integrującego wykonanego w ramach polsko-niemieckiego projektu Unii Europejskiej i zmodyfikowanego w czasie grantu finansowanego przez Komitet Badań Naukowych.